Performance assessment of onboard and scene-based methods for Airborne Prism Experiment spectral characterization

Petra D'Odorico,[1,*] Luis Guanter,[2] Michael E. Schaepman,[1] and Daniel Schläpfer[3]

[1]Remote Sensing Laboratories, University of Zurich, Winterthurerstrasse 190, CH-8057 Zurich, Switzerland

[2]Atmospheric, Oceanic and Planetary Physics, University of Oxford, Parks Road, OX1 3PU Oxford, UK

[3]ReSe Applications, Langeggweg3, CH-9500 Wil SG, Switzerland

*Corresponding author: petra.dodorico@geo.uzh.ch

Received 4 February 2011; revised 23 May 2011; accepted 17 July 2011;
posted 18 July 2011 (Doc. ID 142221); published 12 August 2011

Accurate spectral calibration of airborne and spaceborne imaging spectrometers is essential for proper preprocessing and scientific exploitation of high spectral resolution measurements of the land and atmosphere. A systematic performance assessment of onboard and scene-based methods for in-flight monitoring of instrument spectral calibration is presented for the first time in this paper. Onboard and ground imaging data were collected at several flight altitudes using the Airborne Prism Experiment (APEX) imaging spectrometer. APEX is equipped with an in-flight characterization (IFC) facility allowing the evaluation of radiometric, spectral, and geometric system properties, both in-flight and on-ground for the full field of view. Atmospheric and onboard filter spectral features present in at-sensor radiances are compared with the same features in reference transmittances convolved to varying instrument spectral configurations. A spectrum-matching algorithm, taking advantage of the high sensitivity of measurements around sharp spectral features toward spectrometer spectral performance, is used to retrieve channel center wavelength and bandwidth parameters. Results showed good agreement between spectral parameters estimated using onboard IFC and ground imaging data. The average difference between estimates obtained using the O_2 and H_2O features and those obtained using the corresponding filter features amounted to about 0.3 nm (0.05 of a spectral pixel). A deviation from the nominal laboratory instrument spectral calibration and an altitude-dependent performance was additionally identified. The relatively good agreement between estimates obtained by the two approaches in similar spectral windows suggests they can be used in a complementary fashion: while the method relying on atmospheric features can be applied without the need for dedicated calibration acquisitions, the IFC allows assessment at user-selectable wavelength positions by custom filters as well as for the system on-ground.

OCIS codes: 280.0280, 110.0110, 300.0300, 120.4640.

1. Introduction

A large variety of imaging spectrometers exists [1], and they are successfully being used to simultaneously retrieve variables from different spheres of the Earth [2]. However, numerous studies evidenced severe inaccuracies in retrieved reflectance and higher level products due to errors in instrument spectral calibration [3–5]. The conversion of at-sensor radiance to physical surface reflectance quantity requires compensating for the presence of the atmosphere and its effects, such as absorption and scattering [6,7]. An erroneous instrument spectral calibration would induce compensation at the wrong wavelengths, causing the appearance of atmospheric residual features in the reflectance spectrum. The subsequent exploitation of the spectral features

0003-6935/11/244755-10$15.00/0

present in the retrieved surface reflectance spectra would also introduce a bias in the further analysis and propagate uncertainties into final products.

Errors in spectral calibration parameters are defined as deviations from the nominal parameter values assigned during previous instrument characterization. Errors may occur as shifts in center wavelengths and/or changes in bandwidth i.e., full width at half-maximum (FWHM) of spectral response functions (SRF) associated with individual detector pixels. For area detectors, a further artifact is caused by a variation in dispersion along the dimension of the entrance slit. This leads to a spectral shift that depends on the pixel location along the cross-dispersion direction of the detector, causing a change in detector smile [8]. Technical limitations of instrument design, mechanical tolerances, vibrations, and changes in instrument temperature and pressure are among the most common causes generating deviations in spectral calibration of pushbroom dispersive airborne and spaceborne systems [4].

Due to the high sensitivity of the measured spectrum to the instrument spectral performance in spectral windows where abrupt radiance changes occur, most of the methods for in-flight spectral characterization of imaging spectrometers are based on the evaluation of sharp absorption features present in given radiance spectra used as a reference [9,10]. Typical strategies for in-flight spectral characterization are broadly divided into two groups. The first compares the position of a spectral feature in the observed spectrum to the position of the same feature in a modeled reference spectrum and calculates model parameters producing the best match [4,10]. The second group builds on the notion that links a smooth reflectance-spectrum appearance with an accurate atmospheric compensation model, which in turn is associated with a valid wavelength calibration [5,9,11]. Hence, it looks for the set of spectral parameters, which, when used as an input in the atmospheric correction, results in the smoothest surface reflectance spectrum. Smoothing techniques work well if instrument spectral deviations are small. For larger band shifts, the operation of smoothing, usually performed by moving average, might fail to remove residual features in the smoothed reference spectrum used as surrogate for the true surface [9,12].

To be able to use feature-matching approaches in the spectral domain, the measured spectrum must have distinguishable features occurring at the spectral resolution limit of the instrument at hand and transferable to a known reference spectrum. When relying solely on image data, the reference spectrum is usually given by the modeled at-sensor radiance [5], transmittance, or irradiance [4] signals containing atmospheric absorption features. When available, onboard spectral calibration sources may provide a valid alternative to image data as well as a useful complement covering spectral regions devoid of atmospheric features; reference signals are then usually diffuser plates' absorption lines or dedicated filter transmittances [13–16].

In this paper, a systematic evaluation and comparison of two independent approaches aimed at instrument in-flight spectral characterization is presented for the first time. The first approach relies on dedicated calibration acquisitions performed with characterization equipment onboard the APEX imaging spectrometer. The second approach uses atmospheric features present in standard ground imaging. The investigation focused on the APEX instrument [17], yet outcomes are considered relevant for other operational and upcoming sensor systems holding onboard characterization equipment, such as the Environmental Mapping and Analysis Program (EnMAP) [18]. Among other existing airborne systems, AVIRIS [16,19] and ROSIS [20] also hold internal characterization sources, both used before and after acquisition of a flight line.

2. Materials and Methods

A. APEX Imaging Spectrometer

APEX is an airborne dispersive pushbroom imaging spectrometer developed by a joint Swiss–Belgian consortium in the frame of the European Space Agency's (ESA) PRODEX (PROgramme de Développement d'EXpériences scientifiques) programme. It is designed to validate and calibrate spaceborne missions and contribute to advanced product development. Table 1 presents an overview of APEX performances.

Table 1. APEX Instrument Performance

Spectral Performance		
	VNIR	**SWIR**
Spectral range	375–983 nm	991–2500 nm
Spectral bands	334 (unbinned), 114 (def. binned)	198
Spectral sampling interval	0.45–7.5 nm	5–10 nm
Spectral resolution (FWHM)	0.7–9.7 nm	6.2–12 nm
Spatial Performance		
Spatial pixels (across track)	1000	
FOV	28°	
IFOV	0.028° (~0.5 mrad)	
Spatial sampling interval (across track)	1.75 m at 3500 m above ground level	
Detector Characteristics		
	VNIR	**SWIR**
Type	CCD	CMOS
Dynamic range	14 bit	13 bit
Pixel size	22.5 μm by 22.5 μm	30 μm by 30 μm
Smile	average $<$ 0.35 pixel	
Keystone (frown)	average $<$ 0.35 pixel	
Coregistration	average $<$ 0.55 pixel	
Other Information		
Data capacity	500 GB on solid state disks	
Data transfer	Spectral frames: 30 MB/s	
Data rate for default configuration	0.4 GB/km (1250 km max.)	

The instrument design (Fig. 1) is a dispersive pushbroom spectrometer acquiring the spectral and across-track domain on area detectors. Imaging is performed through forward motion of the aircraft. The field of view (FOV) is projected by the ground imager onto the spectrometer slit using a path folding mirror. To minimize the polarization sensitivity, a scrambler can be inserted to randomize the polarization of the incoming light at the expense of spatial resolution. A collimator lens group directs the light on the first prism. A dichroic coating separates the short-wave infrared (SWIR) and visible and near-infrared (VNIR) channels. The VNIR channel is then dispersed further using a second prism. The VNIR detector is a commercial charged coupled device (CCD) ranging from 380–1000 nm, as of instrument design. For the SWIR channel, a specific complementary metal oxide semiconductor (CMOS) mercury cadmium telluride detector array was developed ranging from 940–2500 nm. The two spectrometer channels are aligned to minimize the geometric coregistration error.

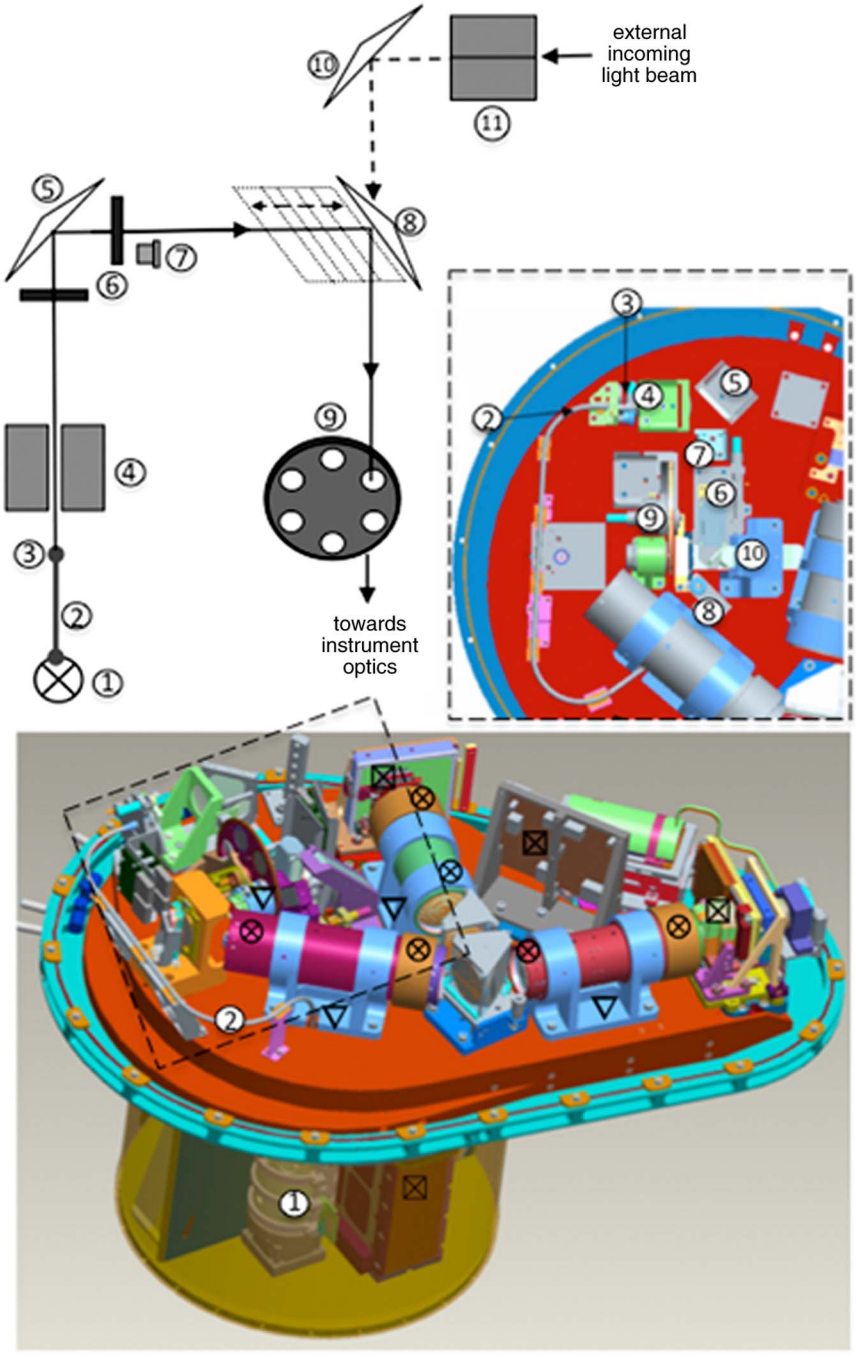

Fig. 1. (Color online) IFC facility onboard APEX: (1) QTH lamp, (2) optical fiber, (3) fiber output (4) calibration shutter, (5) fixed folding mirror, (6) diffusers, (7) feedback loop sensor, (8) sliding folding mirror, (9) filter wheel, (10) fixed folding mirror, (11) global shutter, □ temperature sensor, ∇ temperature sensor on optical base plate (averaged),⊗ differential temperature sensors.

APEX holds an IFC facility (Fig. 1) allowing the characterization of radiometric, spectral, and geometric system properties, both in-flight and on ground covering the full FOV. During in-flight characterization operation, the main instrument shutter is closed to avoid any light penetrating from the outside. A stabilized quartz tungsten halogen (QTH) 75 W lamp in a dedicated housing is attached to an optical fiber. The optical fiber guides the light from the lamp through the calibration shutter, which is usually closed to prevent the IFC light from entering the spectrometer during image acquisition. Diffusers are placed before and after a fixed folding mirror to improve the uniformity of the illumination. A sensor is used to monitor the light level and to control the lamp power accordingly in a closed control loop. A sliding folding mirror is moved into the optical path to reflect the light generated by the IFC toward a filter wheel mounted in front of the ground imager. The wheel holds four spectral filters to be used for instrument spectral stability monitoring, these are three bandpass filters (Spectrogon) with transmission features at 700, 1000, and 2218 nm; and a standard reference material (SRM) filter from the National Institute for Standards and Technology (NIST) holding many distinct absorption features throughout the VNIR and SWIR spectral range. A fifth filter, an NG4 attenuation filter, is used to avoid saturation in the VNIR channel at maximum radiance levels (image acquisition over snow). The sixth filter wheel position is left empty for standard data acquisition. Deterioration of the spectral filters is not expected as they are located inside the enclosed and temperature stabilized optical subunit.

For each filter position, the IFC light is dispersed onto the detectors in exactly the same fashion as ground observations. With this design, the most relevant parameters of APEX's optical performance can be characterized in-flight. IFC measurements will be carried out during each laboratory and flight campaign.

Coregistered onboard with the image and IFC data the system measures environmental parameters, reflecting the state of the instrument during a particular acquisition. For the collection of these housekeeping (HK) data, a number of temperature sensors are placed within the optical subunit (e.g., on both detectors, on the optical base plate) and the baffle compartment (on the power supply unit), while pressure sensors are located inside as well as outside the optical subunit compartment (Fig. 1). In 2009, the recording of HK data coregistered with IFC measurements during targeted on-ground and in-flight experiments allowed identification of a temperature and pressure driven trend on instrument spectral performance. The highest correlation was found with the temperature in the baffle and with the differential pressure [17]. Following these findings an instrument revision took place, aimed at the stabilization of the system for a range of temperature and pressure conditions to be encountered during operation. The revision included the manufacturing of a pressure regulation mechanism for the automatic release or fill-in of nitrogen according to the change in-flight altitude and an optimization of the system heating/cooling regulation.

B. APEX Data

APEX data acquired during a flight campaign in June 2010 were used in this study. APEX has an electronic binning pattern implemented, allowing variable spectral sampling intervals in the 375–616 nm VNIR spectral region for which lower signal-to-noise ratios (SNRs) are expected. In this study, data acquired using the default VNIR binning pattern were used; however, the data analysis focused on spectral regions falling outside of the binned region. A total of 114 and of 198 spectral bands were acquired in this configuration for the VNIR and SWIR, respectively.

Four different flight heights, corresponding to 2500, 3500, 4100, and 6500 m above sea level, were selected based on previous experience suggesting differential pressure and system temperatures having an impact on instrument performance [17]. IFC data were acquired before and after each flight line. The timely proximity of ground imaging and IFC data-takes secured acquisition under comparable environmental conditions verified by means of the coregistered HK data.

Flight lines were flown on consecutive days and slightly differing acquisition times and locations within Switzerland. Simultaneously, vicarious measurements were performed on ground. Before data acquisition, a full laboratory characterization was performed at the Calibration Home Base located at DLR Oberpfaffenhofen in Germany. Laboratory calibration resulted in nominal sensor spectral parameters, i.e., center wavelength and FWHM, measured under controlled conditions. These provided the initial calibration parameters toward which estimates by both in-flight approaches were compared. Data preprocessing included radiometric calibration, spatial resampling, detector coregistration, bad pixel replacement, and a smear correction. For the spectral calibration task, along-track averaging of image data is performed to reduce spatial heterogeneity effects.

C. Estimation of Spectral Parameters

In this study, a methodology was devised aimed at the estimation of instrument spectral parameters (center wavelength and FWHM) by monitoring the position and shape of spectral features, which by nature occur always at the same wavelengths in an APEX spectrum. Three atmospheric absorption features were chosen for the approach relying on ground imaging, these are the O_2-A feature at 760 nm, the H_2O feature at 1135 nm, and the CO_2 feature at 2010 nm. For the IFC-based approach, absorption features were chosen overlapping with atmospheric features as well as in spectral regions devoid of atmospheric features. Figure 2 shows the distribution of spectral features available from the atmosphere and from IFC filters

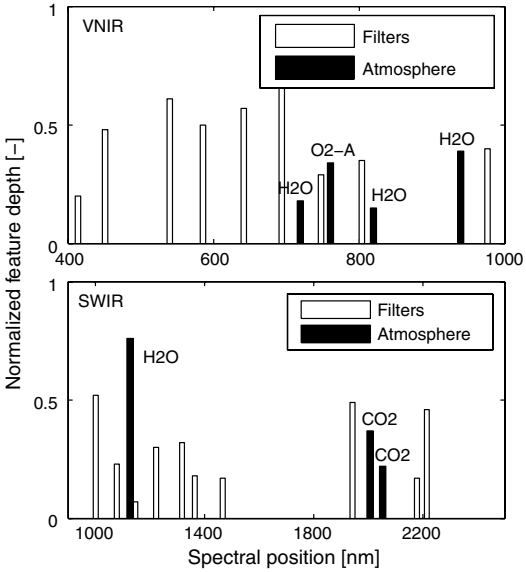

Fig. 2. Position of spectral features of the IFC filters (white) and the atmosphere (black), detectable with APEX spectral resolution. Insufficient signal-to-noise ratio might limit the detectability of some of these features.

mounted on APEX, whose detectability is feasible at APEX's spectral resolution but might still be limited by insufficient SNR (compare [8] for a list of available natural features). The suitability of a feature for the purpose of spectral parameter estimation cannot be determined *a priori*; in this study, features with greater depth were generally preferred. The O_2-A feature is known to hold the greatest potential for spectral characterization because O_2 is very well mixed in the atmosphere and the O_2-A feature is narrow and deep. Absorption features used for the methods' comparison are depicted in Fig. 3.

In the onboard approach, the reference spectrum is given by the transmittance of the SRM filter included in the IFC. The filter characterization is provided by

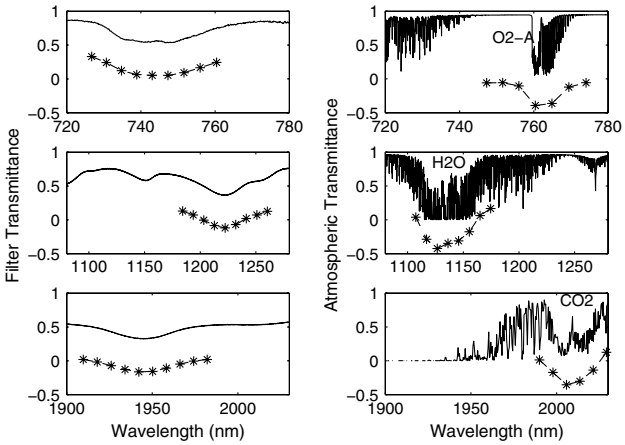

Fig. 3. Absorption features used for VNIR (top) and SWIR (middle, bottom) detectors for instrument spectral parameter estimation. Left: IFC NIST filter features, and right: atmospheric features. The continuous lines show the transmittance spectra while the discontinuous lines represent the same spectra convolved with APEX bands (offset for clarity).

NIST in measurement intervals of 0.1 nm from 350 to 850 nm and 0.25 nm from 850 to 2500 nm.

When using the scene-based approach, a transmittance spectrum is preferred over a radiance spectrum based on the assumption that the shape of atmospheric absorption features in radiance data remains essentially unvaried with respect to the corresponding transmittance spectra. Different studies have favored the former [5,21], others preferred the latter [4], although none of these sources provided clear evidence for the superiority of using one over the other reference. The choice between a generic reference transmittance spectrum and scene-specific ones was made based on a sensitivity analysis investigating the impact of changing atmospheric characteristics on instrument spectral parameters retrieval. Simulations were performed for a simplified scenario, e.g., no instrument noise was assumed and spectral parameters were varied one at a time. Results showed how the influence of varying atmospheric parameterization is merely confined to FWHM estimation and even there it exclusively affected results based on the H_2O and CO_2 features. Large deviations in assumed water vapor content and the derived nonlinearity of the transmittance as a function of it, made it particularly difficult to derive accurate FWHM change estimates using the water vapor feature. The FWHM retrieval based on the latter two features was excluded regardless of these findings due to the insufficient instrument spectral sampling (at 1135 nm: SSI = 9.6 nm; at 2004 nm: SSI = 7.8 nm). A generic transmittance spectrum was found to provide no significant errors for the further analysis and was, therefore, preferred in this study to reduce processing time and efforts associated with the spectral parameter estimation.

The calculation of atmospheric parameters is based on MODTRAN 5 [22], which uses the HITRAN2008 line database [23]. Total upward transmittance ($T^{\uparrow}$) was calculated as the sum of the spectral transmittances for diffuse ($t^{\uparrow}_{\mathrm{dif}}$) and direct ($t^{\uparrow}_{\mathrm{dir}}$) upwelling radiation from the surface to the sensor ($T^{\uparrow} = t^{\uparrow}_{\mathrm{dif}} + t^{\uparrow}_{\mathrm{dir}}$). The direct transmittance is given as a standard MODTRAN output, while the diffuse transmittance can be obtained by a 2-run MODTRAN process as described by Guanter *et al.* [24]. The spectral resolution of the MODTRAN output was set to 8.2 cm^{-1}.

Each reference transmittance spectrum point $T(\lambda_j)$ was convolved with the instrument's calibrated response for those spectral regions encompassing the predefined absorption features (see Fig. 3). Predefined absorption features fall outside the spectral region subject to APEX spectral binning; thus, no pixel binning function needs to be implemented in the convolution. The following equation was used:

$$S_i(\Delta\lambda, \Delta\mathrm{FWHM}) = \sum_{j=1}^{j=N} T(\lambda_j) * \mathrm{SRF}_i(\Delta\lambda, \Delta\mathrm{FWHM}), \quad (1)$$

where $\mathrm{SRF}_i(\Delta\lambda, \Delta\mathrm{FWHM})$ stands for an SRF approximated by a Gaussian function to which a spectral shift ($\Delta\lambda$) and a bandwidth change (ΔFWHM) have been applied and where N is the number of spectral points at which the input reference spectrum was originally sampled.

The convolved transmittances are iteratively fed into an optimization loop, which searches for the band shift and width change that results in the smallest difference between the references and the measured APEX spectra. The optimization is performed based on the Nelder–Mead simplex algorithm as described in Lagarias *et al.* [25]. In order to achieve the best sensitivity, the best match is evaluated using correlation analysis in the region of the absorption features. Features in both the reference and the measured spectrum are continuum normalized assuming a linear continuum. Changes to the spectral parameters fed into the convolution are defined with respect to the initial parameter grids coming from the laboratory characterization. The search uses zero as a starting deviation value for both parameters without upper constraining thresholds for the magnitude of deviations. In few cases, the process ended before the function converged into its optimal value and corresponding estimates were thus removed from the final output.

3. Results and Discussion

A. Spectral Parameters Estimation

Results of the APEX spectral parameter estimation for selected acquisitions are presented in this section. For each detector, we first cross-validated estimates obtained for the same wavelength region using IFC filter features and corresponding atmospheric features. Next, the linearity of retrieved shifts over the detector's spectral dimension was investigated using IFC filter features at different wavelength positions. This second set of results is meant to assess whether the spectral shift derived by one single wavelength position can be used to update the entire spectral range. Estimates obtained with the IFC for the instrument on-ground, before and after the flight, are also presented.

Figure 4 shows the nominal versus the updated smile profiles obtained over four flight altitudes for the VNIR band centered at 760 nm. Estimations based on the O_2-A and corresponding NIST filter feature yield comparable results, differing in average of 0.3 nm, corresponding to 0.05 of a spectral pixel in this particular wavelength region. A deviation from the nominal instrument spectral calibration and an altitude-dependent performance are evident, confirming the unsolved pressure/temperature dependency of the system. For prism-based instruments as APEX, performance changes with altitude are often connected to pressure-dependant dispersion changes of the prism. Results were remarkably reproducible when the instrument was flown at the same altitude on different dates and sites (figures not included here). In the future, the development of a correction model in function of flight height is thus something worth investigating. System performance estimated at the highest flight altitude of 6.5 km shows the greatest deviation from nominal value. A shift of 4.1 nm (0.70 of a spectral pixel) and 4.4 nm (0.75 of a spectral pixel) for the central detector pixel position was estimated by the onboard-based and scene-based approaches, respectively. An increase in smile is further identified by both approaches. Smile, computed as the greatest difference found between the center wavelength values of two detector pixels, amounts to 1.5 nm (0.26 of a spectral pixel) and 2 nm (0.34 of a spectral pixel) for onboard-based and scene-based estimates, respectively, compared to the 0.6 nm (0.1 of a spectral pixel) nominal value.

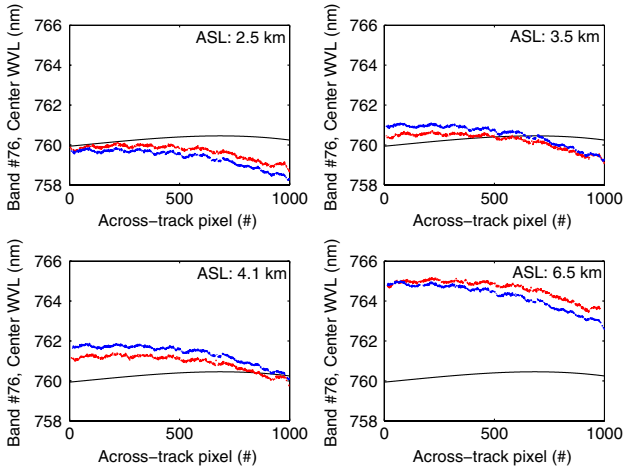

Fig. 4. (Color online) Smile characterization at 760 nm for four flight altitudes. The continuous black line represents the nominal smile as measured in the lab, while the dotted lines represent the estimates based on the O_2-A absorption feature (blue) and on the NIST filter absorption feature (red).

Figure 5 shows a good overlap between estimates based on the three IFC filter features centered at 644 nm, 743 nm, and 803 nm, respectively. For the VNIR detector, the shift estimates in one wavelength region can thus be considered representative for the entire spectral range. Further, measurements taken with the IFC on-ground before and after the flights indicate a good correspondence with the instrument laboratory characterization with across-track spectral shifts close to zero.

For the SWIR detector, two wavelength regions were identified for which NIST-filter and atmospheric features are partly overlapping. Agreement between the estimates obtained with the two approaches is observable in the first of the two examined regions, encompassing the H_2O feature at 1130 nm (Fig. 6). Deviation from nominal performances is greater for the lower of the flown altitude, reaching values of −13 nm, being the equivalent of 1 spectral pixel in this particular wavelength region featuring FWHM of about 12 nm. Values refer to the position of the central detector pixel. A shift amounting to −2 nm (0.17 of a spectral pixel) is estimated

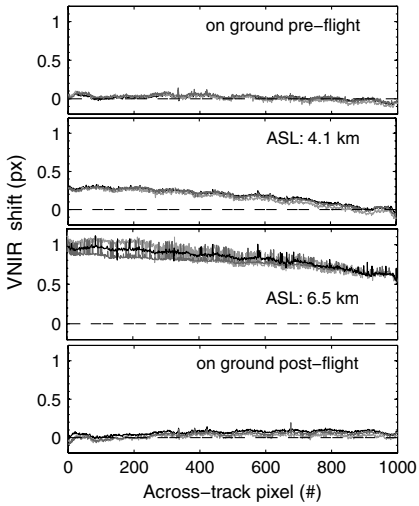

Fig. 5. Estimated spectral shift in the across-track direction expressed as fraction of spectral pixel. Retrieval based on IFC data acquired on ground before (top) and after (bottom) the flight, as well as for two different flight heights. Three VNIR wavelength regions are considered: 630–658 nm (black), 726–760 nm (light gray), 788–819 nm (dark gray).

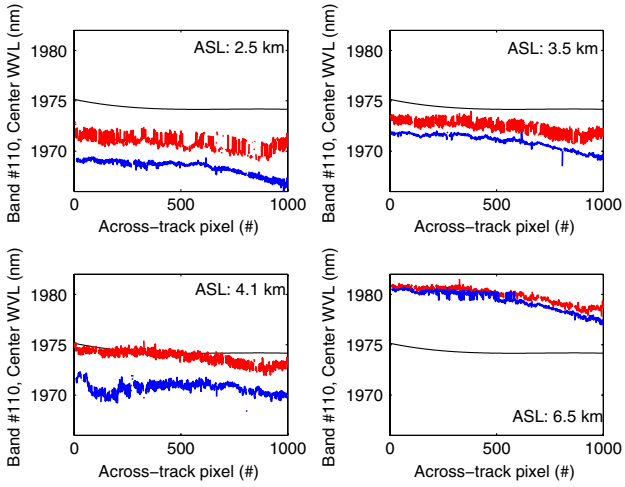

Fig. 7. (Color online) Smile characterization at 1974 nm for four flight altitudes. The continuous black line represents the nominal smile as measured in the lab, while the dotted lines represent the estimates based on the CO_2 absorption feature centered at 2004 nm (blue) and a NIST filter absorption feature centered at 1934 nm (red).

when the system is flown at 6.5 km. The smile for the investigated spectral region amounts to 2 nm (0.17 of a spectral pixel) and 3 nm (0.25 of a spectral pixel) for onboard-based and scene-based estimates, respectively, compared to the 1 nm (0.08 of a spectral pixel) nominal value found in laboratory conditions. In the second SWIR region, estimations based on the CO_2 feature at 2001 nm and analogous NIST-filter feature, confirmed the general direction of the shift evidenced in the former SWIR region, with shifts going from shorter to higher wavelengths with increasing flight altitude (Fig. 7), but significantly differed in magnitude. Smile profiles are characterized by a noisy appearance in the across-track direction particularly for the IFC-based estimates. The two approaches yield estimates diverging in average by 2 nm (0.2 of a spectral pixel), with the exception of the flight performed at the highest altitude for which a nearly perfect overlap of smile profiles is provided. The low at-sensor signal within this absorption feature and the overlap between water vapor and CO_2 absorption (double feature) may have led to the less stable parameter retrieval.

Estimates for three IFC SWIR features confirmed and added to these findings. Results in Fig. 8 show that the two IFC NIST features at 1381 nm and 1934 nm provide concurring shift estimates, while those based on the feature at 1222 nm systematically

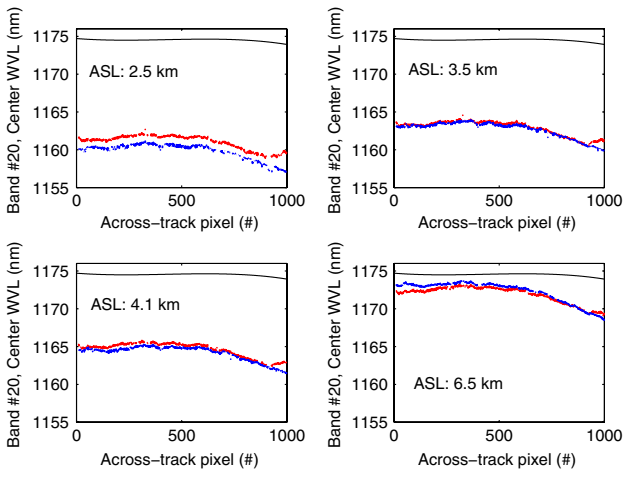

Fig. 6. (Color online) Smile characterization at 1175 nm for four flight altitudes. The continuous black line represents the nominal smile as measured in the lab, while the dotted lines represent the estimates based on the water vapor absorption feature centered at 1130 nm (blue) and a NIST filter absorption feature centered at 1222 nm (red).

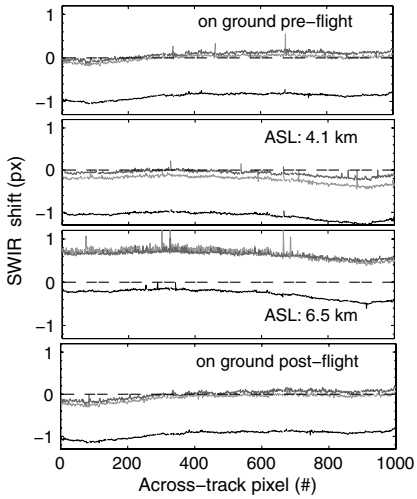

Fig. 8. Estimated spectral shift in the across-track direction expressed as fraction of spectral pixel. Retrieval based on IFC data acquired on ground before (top) and after (bottom) the flight, as well as for two different flight heights. Three SWIR wavelength regions are considered: 1193–1269 nm (black), 1339–1423 nm (light gray), and 1909–1974 nm (dark gray).

diverge by 1 spectral pixel. This holds true as well when on-ground IFC data are considered, thus ruling out the possibility of nonlinear spectral shifts affecting the SWIR detector during flight. Targeted measurements are planned for the next laboratory characterization to help identify the causes of these observations. A faulty instrument laboratory characterization or inaccuracies in the NIST SRM filter characterization in the 1193–1269 nm SWIR region are only two possible hypotheses.

The estimation of the FWHM change in addition to the center wavelength shift in a single inversion step is only recommended if an adequate number of spectral bands, sampling the absorption feature, was provided. A spectral sampling interval (SSI) of 5 nm has been identified as the threshold value above which the number of bands might result insufficient for the inversion of two parameters. For the same reason the impact of not updating the nominal FWHM would not be significant for this type of data [26]. These considerations automatically lead to the exclusion of the FWHM estimation for the SWIR region characterized by SSI ranging between 5–10 nm. For the investigated VNIR region around 760 nm the SSI varies between 3.8 and 4.6 nm and is thus bordering useful limit conditions. Figure 9 presents the nominal FWHM for the VNIR band centered at 760 nm compared to the updates provided by means of the onboard-based and scene-based approaches. It is readily observable that the estimates obtained by the two approaches disagree between each other as well as with the nominal reference. The O_2-A feature provides a less noisy estimate in the across-track direction, which, however, deviates immediately from the nominal FWHM. On the other hand, the IFC filter feature, despite the noise, follows the trend of the ground calibration measurements at low altitude and deviates only for higher altitude. Based on these estimates and those obtained by other IFC filter features (results not shown here) it is not possible to draw any definitive conclusion on changes affecting the FWHM parameter. The insufficient instrument spectral resolution was hypothesized to be among the reasons why an accurate FWHM change retrieval could not be devised.

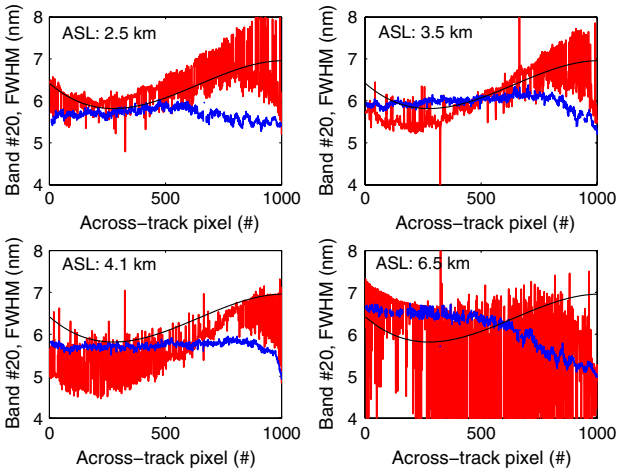

Fig. 9. (Color online) FWHM characterization at 760 nm for four flight altitudes. The continuous black line represents the nominal FWHM as measured in the lab, while the discontinuous lines represent the estimates based on the O_2-A absorption feature (blue) and on the corresponding NIST filter absorption feature (red).

B. APEX Spectral Calibration Updates Verification

The validity of APEX spectral calibration update was verified using a simple atmospheric correction equation. The MODTRAN 5 code was used to compute the different atmospheric parameters required to convert a radiance signal into a reflectance signal [22]. Scene-specific parameterization and a 2-MODTRAN run (see [24]) were needed for this purpose. Reflectances obtained assuming the nominal and the updated spectral calibration are compared. The IFC filter absorption feature around 743 nm was used for updating the VNIR spectral calibration, after previous analysis had shown that the spectral characterization derived from one single spectral position is representative of the entire spectral range covered by the detector. This could not be demonstrated for the SWIR detector, for which a disagreement between estimates was found when using features at different wavelength positions. As a consequence the update of spectral calibration parameters is performed separately for each SWIR spectral region corresponding to an IFC filter feature. Results for the scene acquired at a flight altitude of 6.5 km are shown in Fig. 10 for VNIR and SWIR regions, respectively. Different targets (vegetation, gravel) were selected from the scene, each corresponding to a different across-track position on the detector. The overall perception is that spectra obtained by assuming the updated instrument parameters during atmospheric correction are much smoother than those

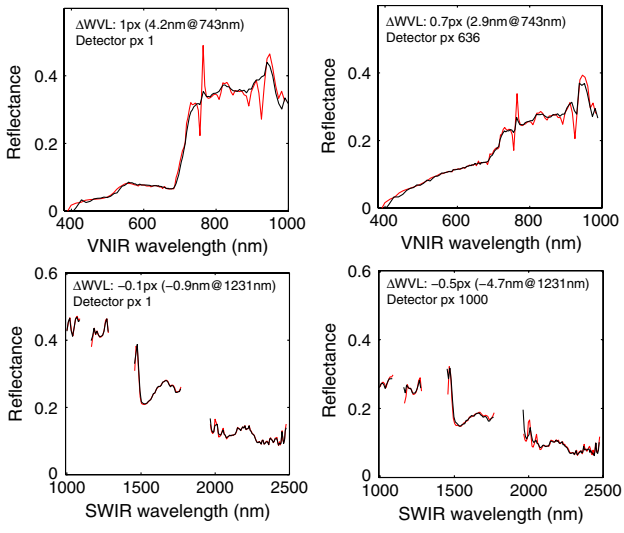

Fig. 10. (Color online) Surface reflectance spectra obtained based on nominal (red) and updated (black) spectral calibration parameters. For the VNIR the update is based on the IFC feature located around 743 nm. For the SWIR the update was performed for each spectral region separately based on the corresponding IFC feature.

derived based on the laboratory spectral calibration. For the VNIR region, the absence of spikes around the O_2-A band, when the updated instrument parameters are assumed, further validates the correctness of the new spectral calibration. Remaining spikes around 940 nm could be explained by water vapor residuals and uncertainties in the radiometric calibration. In the SWIR region, while major error spikes caused by the spectral miscalibration were eliminated, few residual spikes and dips are still present most likely due to an inaccurate water vapor column estimate. However, findings for the SWIR remain to be proven by further measurements and analysis as discussed in Section 3.A.

4. Conclusions and Outlook

In this paper, a systematic analysis of both atmospheric-based and onboard approaches to spectral characterization is presented for the first time. Both approaches rely on the same feature-matching technique and are aimed at improving APEX in-flight spectral calibration. Deviations of instrument spectral parameters are estimated in relation to an initial calibration state defined during laboratory characterization. The hypothesis is that spectral calibration during flight will deviate from the laboratory calibration and can be updated using the employed methods. The calibration process remains fully independent of an atmospheric correction, which in turn can be used as further validation.

Estimates based on onboard filter features showed good agreement with estimates based on O_2 and H_2O atmospheric absorption features, differing in average of about 0.3 nm (0.05 of a spectral pixel) at the central detector pixel position. Differences might be explained by suboptimal features' shape, method uncertainties, and different sampling frequencies of the reference spectra. Within the second investigated SWIR region, efforts resulted in poorer correspondence between the two methods. Estimates based on the CO_2 feature and its corresponding onboard feature showed disagreement of up to 2 nm (0.2 of a spectral pixel) in this region. Cross sensitivities between the solar function and the absorption of CO_2 and H_2O in the atmospheric model and the laboratory calibration uncertainties in this region can explain the observed disagreement. In addition, results showed an altitude-dependent performance deviation for both detectors. Pressure-dependent dispersion changes are known effects in prism-based instruments and future work will include improved pressure and temperature measurements with sensors placed on the dispersing elements.

Combining onboard and scene data for the in-flight monitoring of spectral calibration holds a number of advantages. Cross-validation of calibration efforts is possible, where sufficient features in the same spectral region exist. Further, spectral filters complementing the number and distribution of atmospheric features allow the monitoring of the full wavelength range. The relatively good agreement between estimates obtained by the two approaches in similar spectral windows suggests they can be used in a complementary fashion: while the method relying on atmospheric features can be applied without the need for dedicated calibration acquisitions, the IFC allows assessment at user-selectable wavelength positions by custom filters as well as for the system on-ground. The latter is also the reason why at comparable performances by the two methods, the IFC should be preferred over more conventional approaches relying on ground imaging and related atmospheric features. In the future, with the manufacturing of materials providing even sharper absorption features, onboard spectral characterization sources are expected to gain even more importance over atmospheric-based approaches, particularly in the SWIR region.

Because of the physical nature of the approach, findings of this study are transferable to other instruments as long as boundary conditions are met (e.g., instrument spectral resolution not exceeding atmospheric line database resolution and availability of onboard sources).

This work was carried out in the framework of the APEX project funded by a European Space Agency (ESA) PRODEX (PROgramme de Développement d'EXpériences scientifiques) contract [15449/01/NL/SFe(IC)]. P. D'Odorico acknowledges the support of a Marie Curie Fellowship awarded in the frame of the Sixth Framework Programme through the Hyper-I-Net network. A special thanks goes to A. Hüni for data collection and technical support and to A. Gonsamo for beneficial discussions. The authors also thank two anonymous reviewers for their valuable comments that contributed to the improvement of this work.

References

1. M. E. Schaepman, "Imaging spectrometers," in *The SAGE Handbook of Remote Sensing*, T. A. Warner, M. D. Nellis, and G. Foody (eds.) (SAGE, 2009), pp. 166–178.
2. M. E. Schaepman, S. L. Ustin, A. J. Plaza, T. H. Painter, J. Verrelst, and S. Liang, "Earth system science related imaging spectroscopy—An assessment," Remote Sens. Environ. **113**, S123–S137 (2009).
3. R. Green, "Spectral calibration requirements for Earth-looking imaging spectrometers in the solar-reflected spectrum," Appl. Opt. **37**, 683–690 (1998).
4. B. C. Gao, M. Montes, and C. Davis, "Refinement of wavelength calibrations of hyperspectral imaging data using a spectrum-matching technique," Remote Sens. Environ. **90**, 424–433 (2004).
5. R. A. Neville, L. Sun, and K. Staenz, "Spectral calibration of imaging spectrometers by atmospheric absorption feature matching," Can. J. Remote Sens. **34**, 29–42 (2008).
6. B.-C. Gao, M. J. Montes, C. O. Davis, and A. F. H. Goetz, "Atmospheric correction algorithms for hyperspectral remote sensing data of land and ocean," Remote Sens. Environ. **113**, S17–S24 (2009).
7. F. C. Seidel, A. A. Kokhanovsky, and M. E. Schaepman, "Fast and simple model for atmospheric radiative transfer," Atmos. Meas. Tech. **3**, 1129–1141 (2010).
8. R. Richter, D. Schläpfer, and A. Müller, "Operational atmospheric correction for imaging spectrometers accounting for

the smile effect," IEEE Trans. Geosci. Remote Sens. **49**, 1772–1780 (2011).
9. L. Guanter, R. Richter, and J. Moreno, "Spectral calibration of hyperspectral imagery using atmospheric absorption features," Appl. Opt. **45**, 2360–2370 (2006).
10. J. Brazile, R. A. Neville, K. Staenz, D. Schläpfer, L. Sun, and K. Itten, "Towards scene-based retrieval of spectral response functions for hyperspectral imagers using Frauenhofer features," Can. J. Remote Sens. **34**, S43–S58 (2008).
11. Z. Qu, B. C. Kindel, and A. F. H. Goetz, "The high accuracy atmospheric correction for hyperspectral data (HATCH) model," IEEE Trans. Geosci. Remote Sens. **41**, 1223–1231 (2003).
12. A. Rodger, "SODA: A new method of in-scene atmospheric water vapor estimation and post-flight spectral recalibration for hyperspectral sensors: Application to the HyMap sensor at two locations," Remote Sens. Environ. **115**, 536–547 (2011).
13. S. Delwart, R. Preusker, L. Bourg, R. Santer, D. Ramon, and J. Fischer, "MERIS in-flight spectral calibration," Int. J. Remote Sens. **28**, 479–496 (2007).
14. H. Montgomery, N. Che, K. Parker, and J. Bowser, "The algorithm for MODIS wavelength on-orbit calibration using the SRCA," IEEE Trans. Geosci. Remote Sens. **38**, 877–884 (2000).
15. P. S. Barry, J. Shepanski, and C. Segal, "Hyperion on-orbit validation of spectral calibration using atmospheric lines and an on-board system," Proc. SPIE **4480**, 231–235 (2002).
16. T. Chrien, M. Eastwood, R. Green, C. Sarture, H. Johnson, C. Chovit, and P. Hajek, "Airborne visible/infrared imaging spectrometer (AVIRIS) onboard calibration system," in *Proceeding of the Fifth Annual JPL Airborne Earth Science Workshop* (Jet Prop. Lab., 1995), pp. 31–32.
17. P. D'Odorico, E. Alberti, and M. Schaepman, "In-flight spectral performance monitoring of the Airborne Prism Experiment," Appl. Opt. **49**, 3082–3091 (2010).
18. B. Sang, J. Schubert, S. Kaiser, V. Mogulsky, C. Neumann, K. P. Forster, S. Hofer, T. Stuffler, H. Kaufmann, A. Muller, T. Eversberg, and C. Chlebek, "The EnMAP hyperspectral imaging spectrometer: instrument concept, calibration, and technologies," in *Imaging Spectrometry XIII* (SPIE, 2008), 708605–708615.
19. R. Green, M. Eastwood, C. Sarture, T. Chrien, M. Aronsson, B. Chippendale, J. Faust, B. Pavri, C. Chovit, M. Solis, M. Olah, and O. Williams, "Imaging Spectroscopy and the Airborne Visible/Infrared Imaging Spectrometer (AVIRIS)," Remote Sens. Environ. **65**, 227–248 (1998).
20. S. Thiemann, P. Strobl, P. Gege, N. Stahl, W. Mooshuber, and H. van der Piepen, "Das abbildende spektrometer ROSIS," in *Publikationen der Deutschen Gesellschaft für Photogrammetrie und Fernerkundung*, E. Seyfert (ed.) (DLR, 2001), pp. 147–153.
21. R. O. Green, "Determination of the in-flight spectral calibration of AVIRIS using atmospheric absorption features," in *Proceedings of the Fifth Annual JPL Airborne Earth Science Workshop*, Vol. 1, R. O. Green, ed. (Jet Prop. Lab., 1995), pp. 71–74.
22. A. Berk, G. P. Anderson, P. K. Acharya, L. S. Bernstein, L. Muratov, J. Lee, M. Fox, S. M. Adler-Golden, J. H. Chetwynd, M. L. Hoke, R. B. Lockwood, J. A. Gardner, T. W. Cooley, C. C. Borel, and P. E. Lewis, "MODTRAN 5, a reformulated atmospheric band model with auxiliary species and practical multiple scattering options: Update," Proc. SPIE **5806**, 662–667 (2005).
23. L. S. Rothman, I. E. Gordon, and A. Barbe, "The HITRAN 2008 molecular spectroscopic database," J. Quant. Spectrosc. Radiat. Transfer **110**, 533–572 (2009).
24. L. Guanter, R. Richter, and H. Kaufmann, "On the application of the MODTRAN 4 atmospheric radiative transfer code to optical remote sensing," Int. J. Remote Sens. **30**, 1407–1424 (2009).
25. J. C. Lagarias, J. A. Reeds, M. H. Wright, and P. E. Wright, "Convergence properties of the Nelder–Mead simplex method in low dimensions," SIAM J. Optim. **9**, 112–147 (1998).
26. L. Guanter, K. Segl, B. Sang, L. Alonso, H. Kaufmann, and J. Moreno, "Scene-based spectral calibration assessment of high spectral resolution imaging spectrometers," Opt. Express **17**, 11594–11606 (2009).